Hybrid Multiferroic Behavior in the Double Perovskite $(Ca_{0.5}Mn_{1.5})MnWO_6$

Alexei A. Belik*

Research Center for Materials Nanoarchitectonics (MANA), National Institute for Materials Science (NIMS), Namiki 1-1, Tsukuba, Ibaraki 305-0044, Japan

Abstract

Multiferroic materials with ordered electric dipoles and magnetic spins attract a lot of attention from viewpoints of applications and fundamental science. Multiferroics are generally classified into type-I, where (anti)ferroelectric and magnetic transitions are well separated and have completely different origins, and type-II, where magnetic structures break crystallographic inversion symmetry. Type-III multiferroics were recently introduced, which are close to type-I, but they do not show non-polar-to-polar structural transitions as polar structures are fixed by chemical order. In this work, we describe dielectric and magnetic behaviors observed in the double perovskites, $(Ca_{0.5}Mn_{1.5})MnWO_6$ and $(Ca_{0.3}Mn_{1.7})MnWO_6$, crystallizing in space group $P2_1/n$. Dielectric constant of these compounds showed a peak at T_C = 22 K and T_C = 27 K, respectively, and followed the Curie-Weiss law in wide temperature ranges between T_C and 300 K, where T_C is an (anti)ferroelectric transition temperature – this behavior is typical for type-I multiferroics with proper (anti)ferroelectric transitions. At the same time, T_C matches with the Néel temperature T_N – this behavior is typical for type-II multiferroics. Therefore, materials with such behavior can be called hybrid multiferroics.

1. Introduction

Materials that have ordered electric dipoles and magnetic spins are in general called multiferroics nowadays[1–4] even though the term was originally introduced only for materials with simultaneous ferroelectric and ferromagnetic orders.[5,6] A revision of the definition was "forced" by the discovery of spin-induced ferroelectric transitions in predominantly antiferromagnetic (AFM) materials.[7] In other words, "anti" properties were added to the definition.[4] After intensive studies, a general classification was introduced with type-I and type-II multiferroics. In type-I multiferroics, a ferroelectric transition occurs at a different temperature than a magnetic transition as they have completely different origins.[1–3] Therefore, the coupling between magnetism and ferroelectricity is usually weak. In type-II multiferroics, a specific order of magnetic spins breaks a crystallographic center of symmetry, and weak spontaneous polarization may appear. Type-II multiferroics can show strong electromagnetic coupling.

Temperature dependence of dielectric constant in type-I multiferroics depends on the nature of a ferroelectric transition, whether it is proper (e.g., $BiFeO_3$) or improper (e.g., $YMnO_3$). And in proper (anti)ferroelectrics, dielectric constant usually follows the Curie-Weiss law above the (anti)ferroelectric Curie temperature (T_C) in a wide temperature range.[8] Dielectric constant peaks at T_C (sometimes with very large values) and then decreases with decreasing temperature. There are examples of materials in which dielectric constant increases with decreasing temperature down to lowest temperatures, for example, in the so-called incipient or quantum ferroelectrics, such as $SrTiO_3$ and related materials.[9,10] In type-II multiferroics, dielectric constant usually slightly decreases with decreasing temperature (or nearly temperature independent), and spin-induced ferroelectric transitions appear as peaks/perturbations on such "background" dielectric curves.

A new term – type-III multiferroics – was recently introduced to emphasize materials that are always polar.[11,12] In other words, polar structures are fixed by chemical orders in them and, therefore, they do not show temperature-driven ferroelectric (or non-polar-to-polar structural) transitions. In many cases, they are not ferroelectric (as polarization cannot be switched by an external electric field), but they are pyroelectric. Magnetic behavior of type-I multiferroics below T_C and behavior of type-III multiferroics should,

in principle, be the same as crystal structures are polar in both cases. We also note that near magnetic transition temperatures, which are usually much lower than T_C, electric polarization of type-I multiferroics can also be unswitchable (similar to proposed type-III multiferroics), and ferroelectric switching is rarely demonstrated in type-II multiferroics, where pyroelectric current measurements are often used to support the appearance of spin-induced spontaneous polarization.

In this work, we investigated dielectric and magnetic properties of the double perovskites, $(Ca_{0.5}Mn_{1.5})MnWO_6$ and $(Ca_{0.3}Mn_{1.7})MnWO_6$, which crystallize in space group $P2_1/n$. Dielectric constant of these compounds increased with decreasing temperature and followed the Curie-Weiss law (with a negative Curie-Weiss temperature) from 300 K down to T_C = 22 K ($(Ca_{0.5}Mn_{1.5})MnWO_6$) and T_C = 27 K ($(Ca_{0.3}Mn_{1.7})MnWO_6$); this behavior is typical for proper ferroelectric or antiferroelectric transitions. At T_C, characteristic peaks were observed on dielectric constant. At the same time, T_C matches with the Néel temperature T_N that is typical for type-II multiferroics. We suggest calling materials with such behavior as hybrid multiferroics.

2. Experimental Section

$(Ca_{2-x}Mn_x)MnWO_6$ samples with x = 1, 1.5, 1.7, 1.75, 1.9, and 2 were prepared from stoichiometric mixtures of $CaWO_4$, MnO (99.9 %), and WO_3 (99.9 %), and a sample with x = 0 was prepared from a stoichiometric mixture of Ca_3WO_6, $CaWO_4$, MnO (99.9 %). The synthesis was performed at about 6 GPa and about 1550 K for 2 h in Au capsules (for x = 0, 1, 1.5, 1.7, and 1.75) and about 1850 K for 1 h in Pt capsules (for x = 1, 1.75, 1.9, and 2) using a belt-type high-pressure instrument. After annealing at 1550 K or 1850 K, the samples were cooled down to room temperature by turning off the heating current, and the pressure was slowly released. Hard pellets of approximate diameter of 5 mm were recovered after opening capsules. Single-phase $CaWO_4$ and Ca_3WO_6 were prepared from stoichiometric mixtures of WO_3 and $CaCO_3$ (99.99 %) by annealing in air at 1430 K for 60 h with several intermediate grindings.

X-ray powder diffraction (XRPD) data were collected at room temperature on a RIGAKU MiniFlex600 diffractometer using CuKα radiation (2θ range of 8–100°, a step width of 0.02°, and scan speed of 2 °/min). Synchrotron XRPD data were collected at

room temperature on the beamline BL02B2[13] of SPring-8 (the intensity data were taken between 1.95° and 78.09° at 0.006° intervals in 2θ using a wavelength of λ = 0.619743 Å). The sample was placed into an open Lindemann glass capillary tube (inner diameter: 0.2 mm), which was rotated during measurements. The Rietveld analysis of all XRPD data was performed using the *RIETAN-2000* program.[14]

Magnetic measurements were performed on a SQUID magnetometer (Quantum Design, MPMS3) between 2 and 300 K in an applied field of 10 kOe under both zero-field-cooled (ZFC) and field-cooled on cooling (FCC) conditions. Isothermal magnetization measurements were performed between −70 and 70 kOe at T = 5 K. Specific heat, C_p, at magnetic fields of 0 Oe and 90 kOe was recorded between 2 and 100 K on cooling by a pulse relaxation method using a commercial calorimeter (Quantum Design PPMS). Dielectric properties were measured using a NOVOCONTROL Alpha-A High Performance Frequency Analyzer between 3 K and 300 K on cooling and heating in a frequency range of 301 Hz and 73.7 kHz and at H = 0 Oe. Silver paste was used as electrodes.

3. Results and Discussion

Structural analysis showed that $(Ca_{0.5}Mn_{1.5})MnWO_6$ crystallized in space group $P2_1/n$ (a = 5.31951(2) Å, b = 5.49798(2) Å, c = 7.75735(3) Å, and β = 90.0315(7)°) with a full rock-salt-type ordering of Mn^{2+} and W^{6+} at the B sites. The refined occupation factors were g(Mn) = 1.002(4) and g(W) = 0.995(3). Ca^{2+} and Mn^{2+} cations are statistically disordered in one A site. Figure 1 shows Rietveld-refinement fits based on room-temperature synchrotron X-ray powder diffraction. The sample contained a small amount of $CaWO_4$ impurity (about 0.7 wt. %). Refined structural parameters and main bond lengths are summarized in Tables 1 and 2. Bond-valence sum (BVS)[15] values agreed with the expected formal oxidation states. The crystal structure of $(Ca_{0.5}Mn_{1.5})MnWO_6$ is illustrated on Figure 2.

A sample with the composition of $(Ca_{0.3}Mn_{1.7})MnWO_6$ also crystallized in space group $P2_1/n$ with a = 5.30061(4) Å, b = 5.48014(5) Å, c = 7.75372(6) Å, and β = 90.0605(12)°. On the other hand, the x = 1.75 sample, prepared at 1550 K, already

contained about 15 weight % of a phase with a structure of the high-pressure modification of Mn_3WO_6[16] and with broadened reflections for a Mn_3WO_6-type phase (plus the sample had a small amount of $MnWO_4$ impurity). The amount of the Mn_3WO_6 phase remained almost the same (about 20 wt. %, but with sharper reflections) after the synthesis of the x = 1.75 sample at 1850 K (plus the sample had a small amount (about 2 wt. %) of $MnWO_4$ impurity). Therefore, the $(Ca_{2-x}Mn_x)MnWO_6$ solid solutions are formed up to about x = 1.7 independent of the annealing temperature. The x = 1.9 and 2 samples crystallized in the Mn_3WO_6-type structure with small amounts (about 2 wt. %) of $MnWO_4$ impurity. The formation of $MnWO_4$ impurity was also observed in the previous work.[16] The x =1 sample was prepared in the $P4_2/n$ modification at 1550 K, and in the $P2_1/n$ modification at 1850 K in agreement with the previous work;[17] both modifications contained small amounts of $CaWO_4$ impurity; in addition, the $P2_1/n$ modification contained a small amount of an admixture of the $P4_2/n$ modification and wise versa.

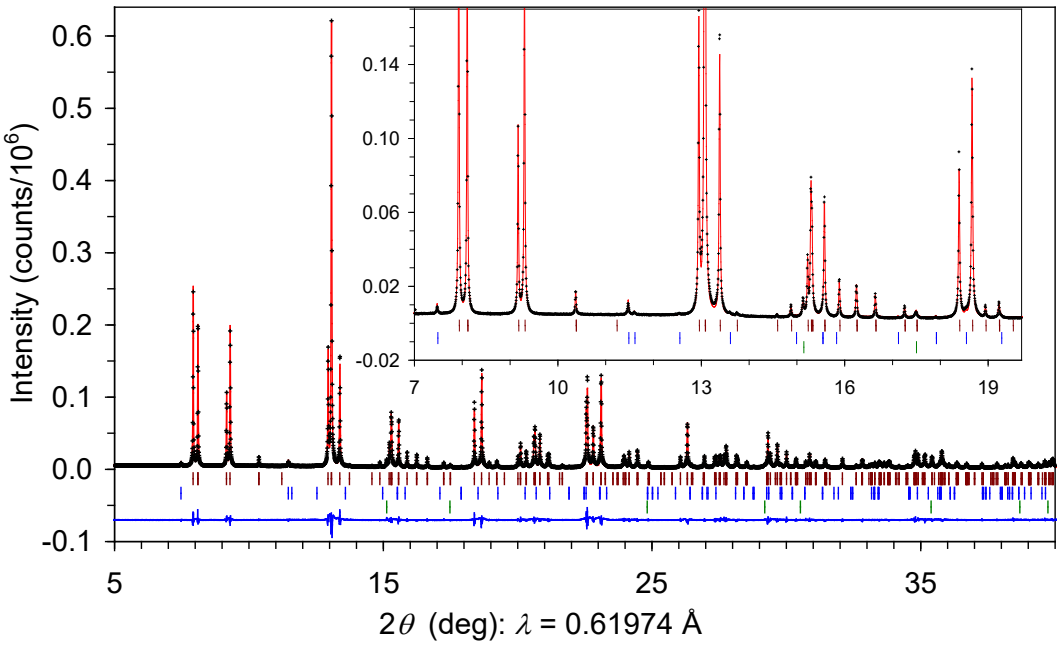

Figure 1. Experimental (black crosses), calculated (red line), and difference (blue line at the bottom) synchrotron X-ray powder diffraction patterns of $(Ca_{0.5}Mn_{1.5})MnWO_6$ at T = 297 K between 5° and 40°. The tick marks show possible Bragg reflection

positions for the main phase, $CaWO_4$ impurity, and Au (a contamination from a capsule material) from top to bottom. Inset shows a zoomed part between 7° and 19.7°.

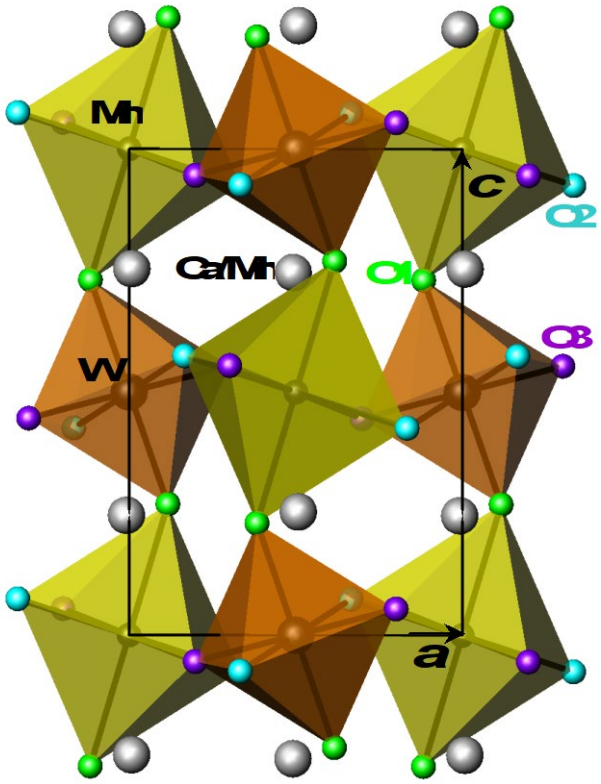

Figure 2. The crystal structure of $(Ca_{0.5}Mn_{1.5})MnWO_6$ viewed along the *b* axis.

Table 1. Refined structural parameters of $(Ca_{0.5}Mn_{1.5})MnWO_6$ at room temperature from synchrotron powder X-ray diffraction data [a]

Site	Wyck.	*x*	*y*	*z*	$B_{iso.}$ (Å^2)
Mn	2*c*	0.5	0.0	0.5	0.71(2)
W	2*d*	0.5	0.0	0.0	0.568(8)
Ca/Mn	4*e*	0.9932(7)	0.0493(2)	0.2466(2)	1.06(3)
O1	4*e*	0.3850(9)	0.9435(10)	0.2301(9)	0.86(14)
O2	4*e*	0.1598(12)	0.2095(12)	0.5697(11)	1.80(19)
O3	4*e*	0.7010(12)	0.3284(11)	0.4474(10)	1.11(15)

[a.] Space group $P2_1/n$ (No. 14, cell choice 2), Z = 2. Wavelength: λ = 0.61974 Å. Occupation factors of the Mn, W, O1, O2, and O3 sites are unity (g = 1); the occupation factor of the Ca/Mn site is 0.25Ca + 0.75Mn. Wyck.: Wyckoff position.

a = 5.31951(2) Å, b = 5.49798(2) Å, c = 7.75735(3) Å, β = 90.0315(7)°, and V = 226.8756(13)Å^3; ρ = 6.400 g/cm^3; R_{wp}= 7.39 %, R_p= 5.41 %, R_B = 3.68 %, and R_F = 2.83 %. Impurities: $CaWO_4$ (0.7 wt. %) and Au (0.5 wt. %; a contamination from a capsule material).

Table 2. Bond lengths (in Å), bond angles (in deg), and bond-valence sum (BVS) in $(Ca_{0.5}Mn_{1.5})MnWO_6$ at room temperature from synchrotron powder X-ray diffraction data.

Ca/Mn–O1	2.168(6)	Mn–O1 ×2	2.203(7)
Ca/Mn–O2	2.172(8)	Mn–O2 ×2	2.213(6)
Ca/Mn–O3	2.192(8)	Mn–O3 ×2	2.138(7)
Ca/Mn–O1	2.269(6)	BVS(Mn^{2+})	+2.08
Ca/Mn–O2	2.605(7)	W–O1 ×2	1.913(7)
Ca/Mn–O3	2.658(7)	W–O2 ×2	1.888(7)
Ca/Mn–O3	2.683(7)	W–O3 ×2	1.894(6)
Ca/Mn–O2	2.800(8)	BVS(W^{6+})	+6.39
BVS(Ca/Mn^{2+})	+1.90	Mn–O1–W ×2	140.84(8)
		Mn–O2–W ×2	137.61(8)
		Mn–O3–W ×2	143.11(8)

BVS = $\sum_{i=1}^{N} v_i$, $v_i = \exp[(R_0 - l_i)/B]$, N is the coordination number, l_i is a bond length, B = 0.37, $R_0(Mn^{2+})$ = 1.79, $R_0(W^{6+})$ = 1.921, $R_0(Ca^{2+})$ = 1.967, and R_0(Ca/Mn^{2+}) = 1.834 (an average of 0.25Ca^{2+} and 0.75Mn^{2+}).[15]

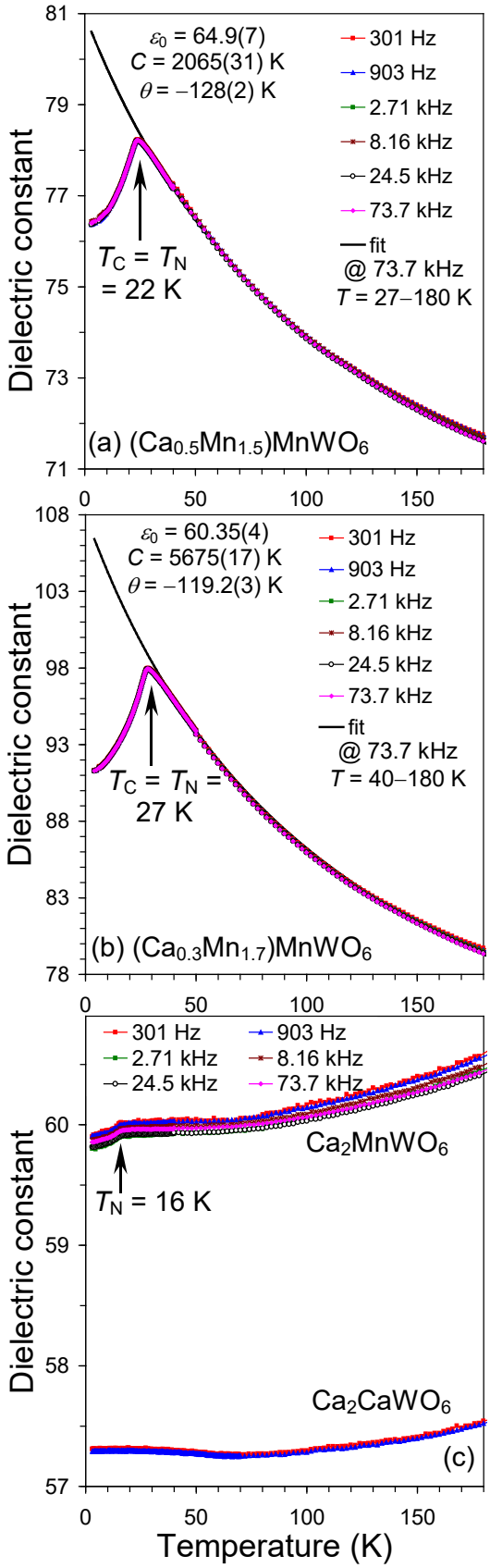

Figure 3. Temperature dependence of dielectric constant of (a) $(Ca_{0.5}Mn_{1.5})MnWO_6$

and (b) $(Ca_{0.3}Mn_{1.7})MnWO_6$ between T = 3 K and 180 K at different frequencies (f) from 301 Hz to 73.7 kHz at zero magnetic field. The black line shows a fit by the Curie-Weiss law (eq. (1)), where the calculated curve was extended down to 3 K; the fitting parameters are given on the figure. T_N: Néel temperature, T_C: (anti)ferroelectric Curie temperature. (c) Temperature dependence of dielectric constant of Ca_2MnWO_6 and Ca_2CaWO_6 (only at 301 Hz and 903 Hz for clarity) between T = 3 K and 180 K.

Temperature dependence of dielectric constant of $(Ca_{0.5}Mn_{1.5})MnWO_6$ is shown on Figure 3a. There was almost no frequency dependence between 3 K and 180 K, and dielectric constant increased with deceasing temperature down to T_C = 22 K. At T_C, a sharp peak was observed typical for a ferroelectric or antiferroelectric transition. Ferroelectric transitions are usually accompanied by peaks on dielectric loss, while antiferroelectric transitions do not show anomalies on dielectric loss.[9,18] No anomalies were observed on dielectric loss in $(Ca_{0.5}Mn_{1.5})MnWO_6$ (Figure S1) suggesting an antiferroelectric transition. Dielectric constant could be fit with the Curie-Weiss law above T_C in a temperature range of 27–180 K:

$$\varepsilon(T) = \varepsilon_0 + C/(T-\theta) \qquad (1).$$

The fitting parameters were ε_0 = 64.9(7), C = 2065(31) K, and θ = –128(2) K (Figure 3a). A negative Curie-Weiss temperature was obtained again pointing to an antiferroelectric transition. Above about 200 K, an upturn of dielectric constant was observed at low frequencies due to increased conductivity and Maxwell-Wagner contributions. However, dielectric constant continued to follow the Curie-Weiss law up to 300 K at high frequencies (Figure S2).

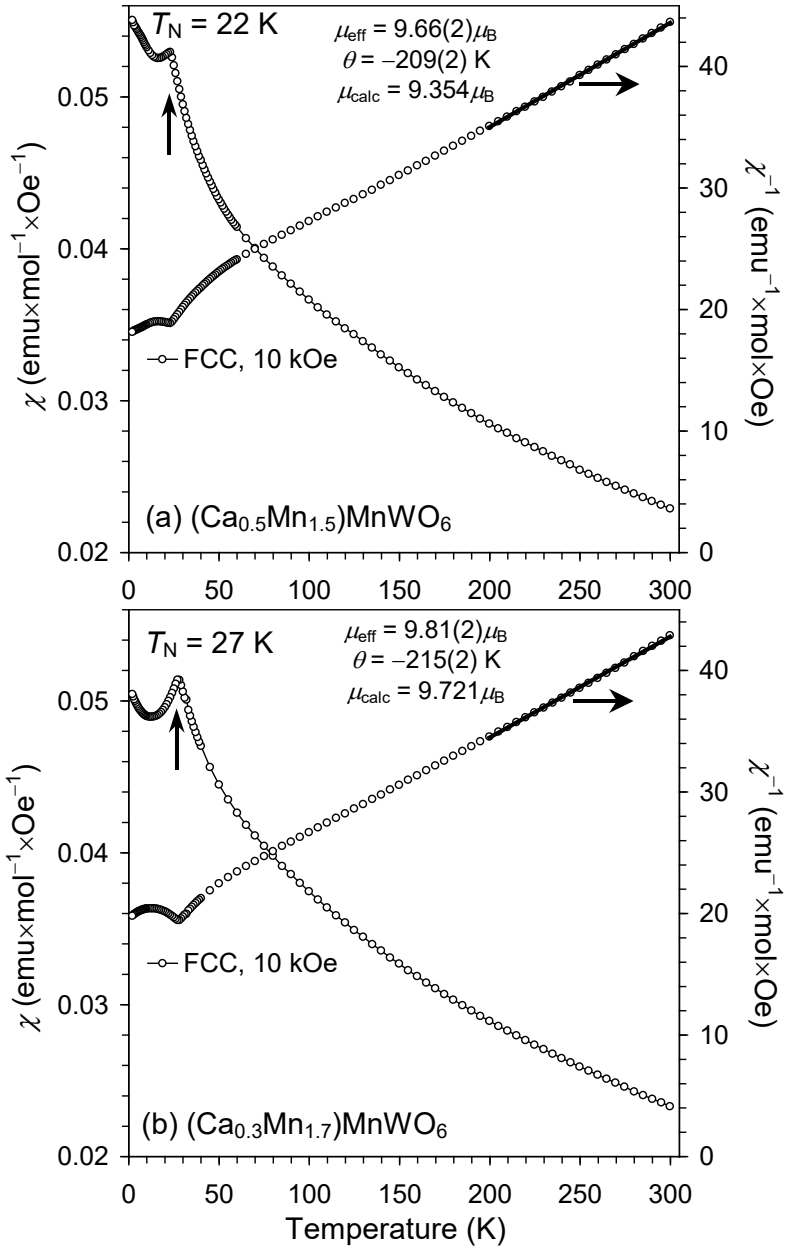

Figure 4. Magnetic properties of (a) $(Ca_{0.5}Mn_{1.5})MnWO_6$ and (b) $(Ca_{0.3}Mn_{1.7})MnWO_6$. The left-hand axis shows a field-cooled on cooling (FCC) dc magnetic susceptibility ($\chi = M/H$) curve measured at H = 10 kOe. Right-hand axis shows the χ^{-1} versus T curve with the Curie-Weiss fit (black line). The parameters of the fit are shown on the figure.

Magnetic properties are reported on Figure 4a. M versus H curves at 5 K showed linear behavior without any detectable hysteresis suggesting pure AFM properties (Figure

S4). Temperature-dependent magnetic susceptibility showed a small peak at T_N = 22 K. At high temperatures, inverse magnetic susceptibilities followed the Curie-Weiss law:

$\chi^{-1}(T) = 8(T-\theta)/\mu_{eff}^2$ (2).

The experimental effective magnetic moment (μ_{eff}) of 9.66μ_B was close to the calculated value of 9.35μ_B, and a negative Curie-Weiss temperature (θ) confirmed predominant AFM interactions. Specific heat measurements (Figure 5) showed a clear peak near 22 K confirming a long-range magnetic ordering.

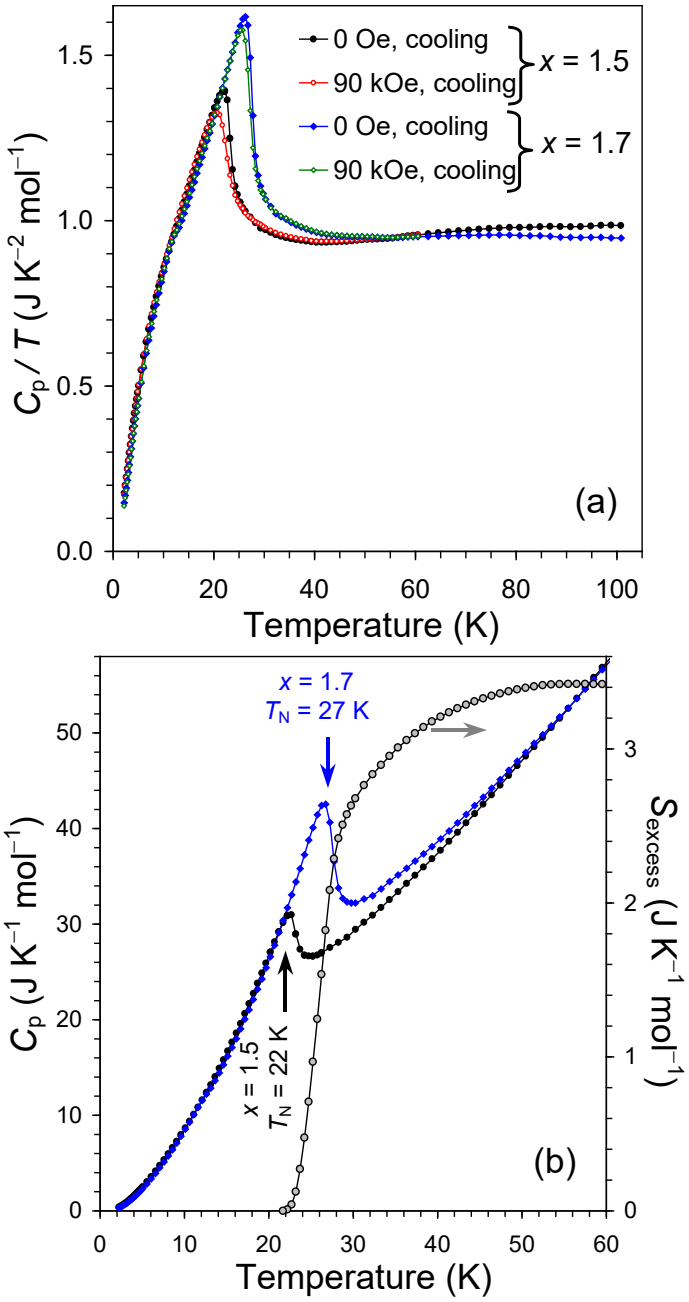

Figure 5. (a) Specific heat data (C_p/T versus T) for $(Ca_{0.5}Mn_{1.5})MnWO_6$ and $(Ca_{0.3}Mn_{1.7})MnWO_6$ at $H = 0$ Oe and 90 kOe. (b) (Left-hand axis) C_p versus T curves for $(Ca_{0.5}Mn_{1.5})MnWO_6$ and $(Ca_{0.3}Mn_{1.7})MnWO_6$ at $H = 0$ Oe. (Right-hand axis) Excess entropy in $(Ca_{0.3}Mn_{1.7})MnWO_6$ in comparison with $(Ca_{0.5}Mn_{1.5})MnWO_6$ at $H = 0$ Oe.

Therefore, magnetic and specific heat data prove that an AFM long-range magnetic transition takes place at the Néel temperature T_N = 22 K. At the same temperature, a clear dielectric constant peak was observed. This is what is usually observed in type-II multiferroics.

A sample with the composition of $(Ca_{0.3}Mn_{1.7})MnWO_6$ was also investigated, and similar dielectric, magnetic, and specific heat anomalies were observed only at a higher temperature of $T_N = T_C$ = 27 K (Figures 3b, 4b, and 5 and Figures S1, S3, and S4). The fit by eq. (1) gave ε_0 = 60.35(4), C = 5675(17) K, and θ = –119.2(3) K. Shifts of both T_N and T_C in $(Ca_{0.3}Mn_{1.7})MnWO_6$ give additional evidence that the transitions take place at the same temperature point. Specific heat of the x = 1.5 and 1.7 samples almost matched each other in temperature ranges of 2–22 K and above about 50 K. The excess entropy of the x = 1.7 sample in comparison with the x = 1.5 sample was calculated to be about 3.4 $J\times mol^{-1}\times K^{-1}$ (Figure 5b), which can approximately be explained by a larger amount of magnetic Mn^{2+} cations ($0.2\times R\times\ln(2S+1) \approx 3.0$ $J\times mol^{-1}\times K^{-1}$, where R is the gas constant and S = 5/2 is spin).

On the other hand, isostructural Ca_2MnWO_6[19,20] (space group $P2_1/n$, a = 5.4564(1) Å, b = 5.6471(1) Å, c = 7.8010(1) Å, and β = 90.202(2)°) showed nearly frequency independent dielectric constant between 2 K and 230 K (Figure 3c and Figure S5), where dielectric constant only very slightly decreased with decreasing temperature without any Curie-Weiss behavior. A very weak kink (not a peak) was observed on dielectric constant at T_N = 16 K; the kink could originate from magnetostriction and magnetodielectric effects.[4] Our specific heat and magnetic measurements of Ca_2MnWO_6 (Figures S6 and S7) confirmed an AFM long-range ordering. Therefore, dielectric properties of isostructural $(Ca_{2-x}Mn_x)MnWO_6$ compounds with x = 0 and x = 1.5 (x = 1.7), having long-range AFM orderings, were quite different. We also investigated dielectric properties of another isostructural compound without magnetic ions, Ca_2CaWO_6[21] (Figure 3c), where dielectric constant was frequency independent between 3 K and 330 K (not shown) and very slightly decreased with decreasing temperature as expected. We note that no dielectric loss anomalies were observed in Ca_2MnWO_6 (Figure S5) and Ca_2CaWO_6.

Table 3. Néel temperatures (T_N) and Parameters of the Curie-Weiss Fit for $(Ca_{2-x}Mn_x)MnWO_6$

x	T_N (K)	μ_{eff} (μ_B/f.u.)	μ_{calc} (μ_B/f.u.)	θ (K)	FI
0	16	5.886(12)	5.916	–61.5(1.3)	3.8
1	8[a)]	8.43(2)	8.367	–158(2)	18[a)]
1.5	22	9.66(2)	9.354	–209(2)	9.5
1.7	27	9.81(2)	9.721	–215(2)	8.0

The Curie-Weiss fits were performed between 200 and 300 K using the FCC χ^{-1} versus T data at 10 kOe. FI: Frustration index = $|\theta|/T_N$. [a)] from Ref. 17, 8 K is a spin-glass temperature.

Previous magnetic measurements and neutron diffraction studies of Ca_2MnWO_6 (x = 0) showed that there is an AFM long-range ordering at T_N = 16 K with the propagation vector of (0, ½, ½).[19,20] The experimental ordered magnetic moment of 4.9μ_B at 1.9 K nearly reached the full expected value of 5μ_B.[19] Despite the full ordered moment and a simple AFM structure Ca_2MnWO_6 has a moderate frustration index (defined as $|\theta|/T_N$) of about 3.8 (Table 3). Ca_2MnWO_6 has only super-super-exchange interactions, Mn–O–(W)–O–Mn, and fully ordered double perovskites with one non-magnetic B cation (and non-magnetic A cations) form a frustrated square-lattice model in general.[22] The frustration index increased in the x = 1.5 and 1.7 samples to about 8–10.

On the other hand, magnetic measurements and neutron diffraction studies of $(CaMn)MnWO_6$ (x = 1) showed the absence of long-range magnetic ordering.[17] This fact shows that the introduction of magnetic Mn^{2+} cations into the A sites enhances spin frustration until some critical concentrations of Mn^{2+} cations. Our specific heat measurements of $(CaMn)MnWO_6$ (Figure S8) confirmed the absence of a long-range magnetic ordering. Dielectric measurements of $CaMnMnWO_6$ (Figure S9) showed nearly frequency- and temperature-independent properties without any Curie-Weiss behavior. Therefore, dielectric properties of isostructural $(Ca_{2-x}Mn_x)MnWO_6$ compounds with x = 1 (without long-range magnetic ordering) and x = 1.5 and 1.7 (with long-range magnetic ordering) were quite different. Higher concentrations of magnetic and small Mn^{2+} cations

at the A site in the x = 1.5 and 1.7 samples could stabilize a new magnetic structure (which yet to be determined in future studies) and result in different behavior.

We note that magnetodielectric effects at AFM ordering transitions with similar (Curie-Weiss-like) dependence of dielectric constant were observed in the literature and explained by spin-phonon coupling without development of ferroelectric order.[4,10,23–27] In case of $BiMn_3Cr_4O_{12}$, it was suggested originally that $T_C \neq T_N$;[26] however, it was showed later that $T_C = T_N$.[27] Explanations provided in the literature do not probably exclude the development of antiferroelectric order (non-polar),[4,10] and spin-phonon coupling cannot explain the Curie-Weiss behavior of dielectric constant far above T_N as observed in $(Ca_{2-x}Mn_x)MnWO_6$ with x = 1.5 and 1.7 and quite different dielectric behavior of isostructural $(Ca_{2-x}Mn_x)MnWO_6$ as a function of the composition. The evolution of dielectric and magnetic properties in $(Ca_{2-x}Mn_x)MnWO_6$ as a function of x is interesting and deserves further studies.

4. Conclusion

In conclusion, double perovskites $(Ca_{0.5}Mn_{1.5})MnWO_6$ and $(Ca_{0.3}Mn_{1.7})MnWO_6$ were prepared by a high-pressure high-temperature method. Their dielectric constant showed a characteristic peak at T_C = 22 K and T_C = 27 K, respectively, and followed the Curie-Weiss law in wide temperature ranges above T_C up to 300 K that is typical for type-I multiferroics with proper ferroelectric (or antiferroelectric) transitions. On the other hand, T_C matched with T_N that is typical for type-II multiferroics. Therefore, we suggest that $(Ca_{0.5}Mn_{1.5})MnWO_6$ and $(Ca_{0.3}Mn_{1.7})MnWO_6$ are examples of materials that can be called hybrid multiferroic materials bearing features of type-I and type-II multiferroics.

Author Information

Corresponding Author

Alexei.Belik@nims.go.jp

Notes

The authors declare no competing financial interest.

Associated Content

Supporting Information

The Supporting information is available free of charge at ….

Figures with detailed dielectric and magnetic properties of $(Ca_{0.5}Mn_{1.5})MnWO_6$, $(Ca_{0.3}Mn_{1.7})MnWO_6$, and Ca_2MnWO_6 (PDF).

Acknowledgements

This work was partially supported by a Grant-in-Aid for Scientific Research (No. JP22H04601) from the Japan Society for the Promotion of Science and the Kazuchika Okura Memorial Foundation (No. 2022-11). Synchrotron radiation was used at the powder diffraction beamline BL02B2 at SPring-8, with permission from the Japan Synchrotron Radiation Research Institute (Proposal Number: 2023B1676). We thank Dr. S. Kobayashi for his help at BL02B2 of SPring-8. MANA is supported by the World Premier International Research Center Initiative (WPI), MEXT, Japan.

References

(1) Tokura, Y.; Seki, S.; Nagaosa, N. Multiferroics of Spin Origin. *Rep. Prog. Phys.* **2014**, *77*, 076501.

(2) Fiebig, M.; Lottermoser, T.; Meier, D.; Trassin, M. The Evolution of Multiferroics. *Nature Rev. Mater.* **2016**, *1*, 16046.

(3) Khomskii, D. Classifying Multiferroics: Mechanisms and Effects. *Physics* **2009**, *2*, 20.

(4) Lawes, G.; Ramirez, A. P.; Varma, C. M.; Subramanian, M. A. Magnetodielectric Effects from Spin Fluctuations in Isostructural Ferromagnetic and Antiferromagnetic Systems. *Phys. Rev. Lett.* **2003**, *91*, 257208.

(5) Schmid, H. Multi-ferroic Magnetoelectrics. *Ferroelectrics* **1994**, *162*, 317–338.

(6) Schmid, H. Some Symmetry Aspects of Ferroics and Single Phase Multiferroics. *J. Phys.: Condens. Matter* **2008**, *20*, 434201.

(7) Kimura, T.; Goto, T.; Shintani, H.; Ishizaka, K.; Arima, T.; Tokura, Y. Magnetic Control of Ferroelectric Polarization. *Nature (London, U. K.)* **2003**, *426*, 55−58.

(8) Kamba, S. Soft-mode Spectroscopy of Ferroelectrics and Multiferroics: A Review. *APL Mater.* **2021**, *9*, 020704.

(9) Kamba, S.; Savinov, M.; Laufek, F.; Tkac, O.; Kadlec, C.; Veljko, S.; John, E. J.; Subodh, G.; Sebastian, M. T.; Klementova, M. *et. al.* Ferroelectric and Incipient Ferroelectric Properties of a Novel $Sr_{9-x}Pb_xCe_2Ti_{12}O_{36}$ (x = 0–9) Ceramic System. *Chem. Mater.* **2009**, *21*, 811–819.

(10) Katsufuji, T.; Takagi, H. Coupling Between Magnetism and Dielectric Properties in Quantum Paraelectric $EuTiO_3$. *Phys. Rev. B* **2001**, *64*, 054415.

(11) Ravi Shankar, P. N.; Swarnamayee, M.; Sundaresan, A. Polar Magnetic Oxides from Chemical Ordering: A New Class of Multiferroics. *APL Mater.* **2020**, *8*, 040906.

(12) Mishra, S.; Yanda, P.; Orlandi, F.; Manuel, P.; Koo, H.-J.; Whangbo, M.-H.; Sundaresan, A. Contrasting Magnetic and Magnetoelectric Properties of $LuMWO_6$ (M = Fe and Cr): Role of Spin Frustration and Noncollinear Magnetic Structure. *Phys. Rev. B* **2023**, *108*, 014435.

(13) Kawaguchi, S.; Takemoto, M.; Osaka, K.; Nishibori, E.; Moriyoshi, C.; Kubota, Y.; Kuroiwa, Y.; Sugimoto, K. High-throughput Powder Diffraction Measurement System Consisting of Multiple MYTHEN Detectors at Beamline BL02B2 of SPring-8. *Rev. Sci. Instrum.* **2017**, *88*, 085111.

(14) Izumi, F.; Ikeda, T. A Rietveld-analysis Program RIETAN-98 and its Applications to Zeolites. *Mater. Sci. Forum* **2000**, *321–324*, 198–205.

(15) Brese, N. E.; O'Keeffe, M. Bond-valence Parameters for Solids. *Acta Crystallogr., Sect. B: Struct. Sci*. **1991**, *47*, 192–197.

(16) Li, M.-R.; McCabe, E. E.; Stephens, P. W.; Croft, M.; Collins, L.; Kalinin, S. V.; Deng, Z.; Retuerto, M.; Gupta, A. S.; Padmanabhan, H. *et. al.* Magnetostriction-polarization Coupling in Multiferroic Mn_2MnWO_6. *Nat. Comm.* **2017**, *8*, 2037.

(17) Ji, K.; Alharbi, K. N.; Solana-Madruga, E.; Moyo, G. T.; Ritter, C.; Attfield, J. P. Double Double to Double Perovskite Transformations in Quaternary Manganese Oxides. *Angew. Chem. Int. Ed.* **2021**, *60*, 22248–22252.

(18) Stefanovich, S. Yu.; Belik, A. A.; Azuma, M.; Takano, M.; Baryshnikova, O. V.; Morozov, V. A.; Lazoryak, B. I.; Lebedev, O. I.; Van Tendeloo, G. Antiferroelectric Phase Transition in $Sr_9In(PO_4)_7$. *Phys. Rev. B* **2004**, *70*, 172103.

(19) Munoz, A.; Alonso, J. A.; Casaisq, M. T.; Martinez-Lope, M. J.; Fernandez-Diaz, M. T. Crystal and Magnetic Structure of the Complex Oxides Sr_2MnMoO_6, Sr_2MnWO_6 and Ca_2MnWO_6: a Neutron Diffraction Study. *J. Phys.: Condens. Matter* **2002**, *14*, 8817–8830.

(20) Azad, A. K.; Ivanov, S. A.; Eriksson, S.-G.; Eriksen, J.; Rundlof, H.; Mathieu, R.; Svedlindh, P. Nuclear and Magnetic Structure of Ca_2MnWO_6: A Neutron Powder Diffraction Study. *Mater. Res. Bull.* **2001**, *36*, 2485–2496.

(21) Day, B. E.; Bley, N. D.; Jones, H. R.; McCullough, R. M.; Eng, H. W.; Porter, S. H.; Woodward, P. M.; Barnes, P. W. Structures of Ordered Tungsten- or Molybdenum-containing Quaternary Perovskite Oxides. *J. Solid State Chem.* **2012**, *185*, 107–116.

(22) Mustonen, O.; Vasala, S.; Mutch, H.; Thomas, C. I.; Stenning, G. B. G.; Baggio-Saitovitch, E.; Cussen, E. J.; Karppinen, M. Magnetic Interactions in the $S = 1/2$ Square-Lattice Antiferromagnets Ba_2CuTeO_6 and Ba_2CuWO_6: Parent Phases of a Possible Spin Liquid. *Chem. Comm.* **2019**, *55*, 1132−1135.

(23) Lawes, G.; Kimura, T.; Varma, C. M.; Subramanian, M. A.; Rogado, N.; Cava, R. J.; Ramirez, A. P. Magnetodielectric Effects at Magnetic Ordering Transitions. *Prog. Solid State Chem.* **2009**, *37*, 40–54.

(24) Pal, A.; Huang, C. H.; Yen, T. W.; Lee, P. H.; Chang, Y. H.; Yeh, C. H.; Kuo, T. W.; Tiwari, A.; Chandrasekhar Kakarla, D.; Huang, S. M. *et. al.* Spin-induced Strongly Correlated Magnetodielectricity, Magnetostriction Effect, and Spin-phonon Coupling in Helical Magnet $Fe_3(PO_4)O_3$. *Phys. Rev. B* **2022**, *106*, 094404.

(25) Zhao, L.; Dalton, C.; Liao, S.-C.; Hu, Z.; Lin, H.-J.; Chen, C.-T.; Komarek, A. C. Single Crystal Growth and Physical Properties of Dolerophanite Single Crystals. *Phys. Rev. Mater.* **2019**, *3*, 124403.

(26) Zhou, L.; Dai, J. H.; Chai, Y. S.; Zhang, H. M.; Dong, S.; Cao, H. B.; Calder, S.; Yin, Y. Y.; Wang, X.; Shen X. D. *et al.* Realization of Large Electric Polarization and Strong Magnetoelectric Coupling in $BiMn_3Cr_4O_{12}$. *Adv. Mater.* **2017**, *29*, 1703435.

(27) Maia, A.; Kadlec, C.; Savinov, M.; Vilarinho, R.; Moreira, J. A.; Bovtun, V.; Kempa, M.; Míšek, M.; Kaštil, J.; Prokhorov, A. *el al.* Can the Ferroelectric Soft Mode Trigger an Antiferromagnetic Phase Transition? *J. Eur. Ceram. Soc.* **2023**, *43*, 2479−2487.

For Table of Contents Only

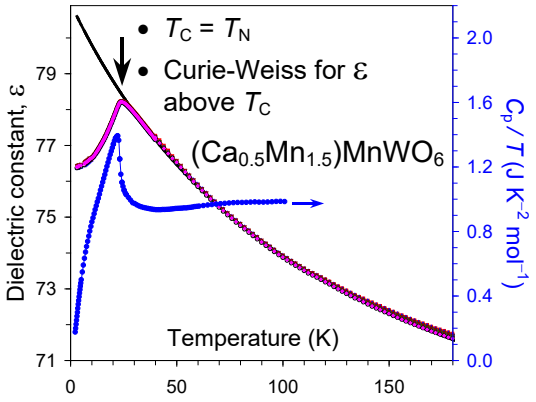

Dielectric and magnetic properties of the double perovskite $(Ca_{0.5}Mn_{1.5})MnWO_6$ give a basis to introduce a term "hybrid multiferroics", where features of type-I and type-II multiferroics are combined.